# A coupled photo-piezo-catalytic effect in a BST-PDMS porous foam for enhanced dye wastewater degradation

Suwen  $Xu^{1,2,\perp}$ , Weiqi Qian<sup>1,4,\perp}</sup>, Ding Zhang<sup>1,4</sup>, Xue Zhao<sup>1</sup>, Xiaoming Zhang<sup>2</sup>, Chuanbo  $Li^{2,*}$ , Chris R. Bowen<sup>3</sup>, Ya Yang<sup>1,4,5,\*</sup>

<sup>1</sup>CAS Center for Excellence in Nanoscience, Beijing Key Laboratory of Micro-Nano Energy and Sensor, Beijing Institute of Nanoenergy and Nanosystems, Chinese Academy of Sciences, Beijing 100083, P. R. China.

<sup>2</sup>College of Life and Environmental Sciences; School of Science; Optoelectronics Research Center, Minzu University of China, Beijing 100081, P. R. China.

<sup>5</sup>Center on Nanoenergy Research, School of Physical Science and Technology, Guangxi University, Nanning 530004, P. R. China.

ABSTRACT: Over the last decade, ferro-/piezo-electric materials have provided new directions to improve catalysis. However, current challenges that must be solved include secondary pollution by the piezoelectric particulates and a limited potential for reuse and recyclability. Here, we report an efficient approach of using a piezoceramic-polymer porous foam to package barium strontium titanate (BST) particulates and prevent secondary pollution, while being able to maintain a high photo-piezo-catalytic performance after 10 cycles of repeated catalytic reactions. The photo-piezo-catalysis achieves a 97.8% dye degradation and an enhanced performance of 275% when compared to individual photocatalysis by light irradiation or periodic low-frequency mechanical squeezing alone. It is suggested the photo-piezo-catalytic coupling effect combines the advantages of increased generated electron-hole pairs and the induced piezoelectric electric field leads to a higher degree of electron-hole separation. The BST-PDMS porous foam for photo-piezo-catalysis offers a potential approach in wastewater degradation via utilizing both solar energy and environmental mechanical sources.

KEYWORDS: coupled photo-piezo-catalytic effect, photocatalysis, piezo-catalysis, piezoelectric effect

<sup>&</sup>lt;sup>3</sup>Department of Mechanical Engineering, University of Bath, BA2 7AK, UK.

<sup>&</sup>lt;sup>4</sup>School of Nanoscience and Technology, University of Chinese Academy of Sciences, Beijing 100049, P. R. China.

<sup>&</sup>lt;sup>1</sup>These authors contributed equally: Suwen Xu, Weiqi Qian

<sup>\*</sup>Correspondence and requests for materials should be addressed to Y. Y. (email: yayang@binn.cas.cn); C. L. (email: cbli@muc.edu.cn).

Today, the combination of the energy crisis and environmental pollution are important scientific challenges that are attracting world-wide attention. This has led to increasing interest in energy harvesting and utilizing clean and renewable energy sources throughout the global scientific community. Solar energy is one of the most ubiquitous, pollution-free and green energy sources, and has been extensively investigated in an effort to convert sunlight into a source of electrical energy. In particular, solar cells and photocatalysis systems have been considered in order to exploit the photovoltaic effect. However, for industrial and practical applications, the rapid recombination of photoinduced electron-hole pairs in conventional semiconductor materials is a significant issue that limits the photovoltaic conversion efficiency, and results in a weak and inefficient photocatalytic reaction. As a result, a series of measures to restrict photoinduced charge recombination have been considered which include operation at an elevated temperature, impurity doping, and creating heterostructures; nevertheless the efficiency continues to be restricted.

In recent decades, ferro-/piezo-electric materials have been found to be promising technologies to drive catalytic reactions with respect to energy and environmental contamination issues. <sup>11-13</sup> It is generally accepted that the piezoelectrically induced built-in electric field across a piezoelectric particle can provide a driving force for the separation of electric carriers, which is termed the *piezo-catalytic* effect. This phenomenon has been used to improve photocatalysis <sup>14,15</sup>; for example Li *et al.* demonstrated that an Ag<sub>2</sub>O-BaTiO<sub>3</sub> hybrid photocatalyst achieved an enhanced photocatalytic activity for Rhodamine B dye degradation under periodic ultrasonic excitation. <sup>16</sup> Mushtaq *et al.* reported an enhanced and efficient degradation of organic pollutants utilizing piezoelectric BiFeO<sub>3</sub> nanosheets and nanowires under visible light irradiation and excitation by mechanical vibrations. <sup>17</sup> Hu and co-workers achieved an enhanced photocatalytic hydrogen evolution using Bi<sub>4</sub>NbO<sub>8</sub>Br. <sup>18</sup>

One potential disadvantage of dispersing particulate-based piezo-catalysts, which are at the nano/micro-scale, in a solution is that they can readily flow into an aqueous environment and act as a secondary form of pollution. The use of fine scale particles in a solution to be treated, such as water, also limits its potential reuse and recyclability, since they must be subsequently collected. Thus, in order to solve the challenges of secondary pollution and reusable limits, Qian *et al.* designed a system of BaTiO<sub>3</sub> particles that were encapsulated in a polydimethylsiloxane (PDMS) matrix to fabricate a porous foam which was able to achieve efficient organic Rhodamine B dye degradation under the action of ultrasonic vibrations. Nevertheless, it is worth noting that there remain challenges since the catalytic reactions weaken over time, which is likely to be due to the fracture of the piezoelectric material under the action of ultrasonic vibrations and the resulting cavitation damage from the high intensity and high

frequency ultrasound. Thus, the application of low frequency and low energy vibrations may provide a route for longer term use of piezoelectric materials for piezo-catalytic reactions.

Lead-free barium strontium titanate (Ba<sub>1-x</sub>Sr<sub>x</sub>TiO<sub>3</sub>) consists of BaTiO<sub>3</sub> and SrTiO<sub>3</sub>, and is a typical perovskite oxide material which possesses excellent ferro-/piezo-electric characteristics. 20-22 The dielectric constant of Ba<sub>1-x</sub>Sr<sub>x</sub>TiO<sub>3</sub> changes with the content of SrTiO<sub>3</sub>, and the dielectric constant reaches a maximum when x = 0.3; the material has also demonstrated significant potential for organic pollutant treatment.<sup>23</sup> In addition, nano-scale materials with ultra-high surface area are able to improve the migration of electric charges between the material and aqueous solution, which is beneficial to enhance electrochemical catalysis.<sup>24,25</sup> In this work, we therefore packaged Ba<sub>0.7</sub>Sr<sub>0.3</sub>TiO<sub>3</sub> (BST) nanoparticles using PDMS to fabricate a BST-PDMS porous foam catalyst and achieve an enhanced photo-piezo-catalytic coupling effect by a combination of light irradiation and low-frequency mechanical squeezing; this can be seen in the Schematic of Fig. 1a. The photo-piezo-catalysis achieved a 97.8% RhB dye degradation and an enhanced catalytic performance of 275% when compared to individual photocatalysis by light only. In addition, photo-piezo-catalytic recycling testing of the BST-PDMS porous foam shows that the degradation efficiency is maintained after repeated catalytic reaction of 10 cycles; from 97.8% at the 1st cycle to 92.7% at the 10th cycle. Moreover, the degradation efficiency and coupling of catalytic effects is examined in detail for a range of BST additive amounts, squeeze frequencies, dye types and operational pH levels. It is suggested the photo-piezo-catalytic coupling effect combines the advantages of an increased number of generated electron-hole pairs due to the photovoltaic effect and piezoelectric field which achieves a higher efficiency of electron-hole separation. The BST-PDMS porous foam for photo-piezo-catalytic coupling dye degradation offers a potential approach in wastewater degradation via utilizing a combination of solar energy and environmental mechanical sources.

#### **Results**

Characterization of piezoelectric BST and BST-PDMS. The as-prepared BST nanoparticles encapsulated in BST-PDMS are mainly quadrilateral in shape with an average size of 400 nm, as shown in Figure 1b. An SEM image of the prepared BST-PDMS porous foam is illustrated in Figure 1c, where the average diameter of the pores of the BST-PDMS foam are ~200 µm. The porous structure provides a beneficial and ample contact of the piezoelectric BST nanoparticle with dye solutions and limits the potential of secondary pollution by the ferroelectric particles. In addition, the pore size is in the range of hundreds of micrometers and is able to maintain the excellent mechanical properties of foam. Images of a circular geometry BST-PDMS porous foam is shown in Figure 1d and 1e with an average diameter of

~4 cm and a thickness of ~1 cm, which possesses mechanical properties that allow it to be flattened and then return to its original shape under repeated mechanical squeezing. In Figure 1f, the BST-PDMS porous foam is placed in a dye solution with the application of mechanical squeezing at a low frequency of 0.71 Hz under a constant light illumination of 1 sun, which is described as *photo-piezo-catalysis*. Under the action of photo-piezo-catalytic activity of 90 min, the color of the RhB dye degrades and fades gradually from an initial pink colour to a final transparent condition.

In terms of the basic characteristics of the BST material, the phase structure of BST transforms from a cubic to tetragonal below to Curie temperature ( $T_c = \sim 32$  °C), where the spontaneous polarization of the tetragonal perovskite ferroelectric BST results from the displacement polarization of Ti<sup>4+</sup> due to the titanium atom moving away from the center of oxygen octahedron; as outlined Figure 2a. 23,26,27 Typical XRD patterns of the BST nanoparticles can be seen in Figure S1b, where the diffraction peaks at 22.3, 31.7, 39.2, 45.4, 56.6, 66.3 and 75.5° can be indexed to the (100), (101), (111), (002), (211), (202) and (310) planes of the tetragonal perovskite BST (JCPDS No. 44-0093, P4mm), where no impurity diffraction peaks are detected, thereby indicating the prepared BST nanoparticles are ferro-/piezoelectric and exhibit high crystallinity.<sup>28</sup> For further characterisation of the material, Piezo-Force-Microscopy (PFM) was used to analyze the piezoelectricity of the BST nanoparticles in contact mode, where the powders were adhered to a conducting resin on a smooth metal plate. Using a scanning area of  $0.5 \times 0.5 \,\mu\text{m}^2$ , the morphology, vertical piezoresponse amplitude and phase image of the BST nanoparticles are illustrated in Figure 2b-d, respectively. Clear contrast is shown in the vertical piezoresponse amplitude and phase image, which indicates the BST nanoparticles exhibit excellent piezoelectricity with a range of polarization directions. In addition, under a 10 V reversal applied field, local piezoelectric hysteresis loops of the BST nanoparticles are recorded in Figure 2e-f, where the butterfly-shaped displacement-voltage hysteresis loop also proves evidence of ferroelectricity, and the phase angle exhibits an inversion.

Enhanced photo-piezo-catalytic coupling effect. The absorbance intensity (A) of RhB is in proportion to the concentration (C) of the solution due to the Beer-Lambert Law, Equation 1:<sup>29</sup>

$$A = KbC \tag{1}$$

Where *K* and *b* are the molar absorption coefficient and the effective thickness of the absorption layer respectively. The degradation of RhB solution using a BST-PDMS porous foam catalyst exhibits different efficiencies under different excitation conditions, as shown in Figure 3a-c. Within 90 min, the absorbance peak of RhB at 554 nm falls over time which indicates efficient degradation of the dye, where employing photocatalysis alone leads to the degradation rate being relatively slow and weak,

while piezo-catalysis alone achieves an intermediate degradation rate. However, the coupling of both photocatalysis and piezo-catalysis leads to the absorbance peak disappearing completely after 90 min, which indicates a complete degradation of the RhB solution. In addition, images of RhB solution before, during, and after photocatalytic, piezo-catalytic, and photo-piezo-catalytic dye degradation are shown in Figure S2a,b and Figure 1g. The colour of the RhB solution exhibits a limited change before and after photocatalysis alone, but after being subjected to combined photo-piezo-catalysis the RhB solution fades rapidly from an initial pink colour to a final optically transparent condition. To clarify the importance of the BST-PDMS porous foam catalyst in our catalytic experiments, pure PDMS porous foam was also evaluated as a control sample and performed poorly, as seen in Figure 3d, where the symbol  $C_0$  represents the intensity of the absorbance peak of the initial RhB solution. The decomposition ratio, represented by D, can be expressed as the following Equation 2:

$$D = 100\% (1 - C/C_0) \tag{2}$$

The calculated D for photocatalysis, piezo-catalysis, and combined photo-piezo-catalysis are 26.1%, 88.0% and 98.8%, respectively. To assess the durability and stability test of the BST-PDMS porous foam, 10 cycles for repeatable photo-piezo-catalysis are shown in Figure 3f. The calculated D for the 10 cycles indicate almost no decrease from the 1<sup>st</sup> cycle of D = 97.8% to the 10<sup>th</sup> cycle of D = 92.7%, indicating our BST-PDMS porous foam catalyst has excellent re-use and recycling ability. This is in contrast to other work on cyclic catalytic testing, where the calculated D decreases to approximately 50% after 12 cycles; our BST-PDMS porous foam catalyst has a small decrease of 5.1% in efficiency after 10 cycles and thereby offers improved durability and stability.

The influencing factors for photo-piezo-catalysis include the amount of BST additive, squeeze frequency, dye type and pH level and are now taken into consideration in the following section. From Figure 4a, the dependence of D on the additive amount of BST can be observed, where for photocatalysis the value of D initially increases with BST amount and then drops slightly, while for photo-piezo-catalysis the value of D continues to increase with BST additive amount. In addition, the extent of the photo-piezo-catalytic coupling effect, in comparison to photo-catalysis and piezo-catalysis, can be evaluated by Equations 3 and 4:

$$\varepsilon_{1} = \frac{D_{\text{photo-piezo}} - D_{\text{piezo}}}{D_{\text{piezo}}} \times 100\%$$
(3)

$$\varepsilon_2 = \frac{D_{\text{photo-piezo}} - D_{\text{photo}}}{D_{\text{photo}}} \times 100\%$$
 (4)

Where  $\varepsilon_1$  and  $\varepsilon_2$  are the enhancement values for photo-piezo-catalysis compared to piezo-catalysis alone and photo-catalysis alone at the same conditions, respectively. Both  $\varepsilon_1$  and  $\varepsilon_2$ , shown in Figure 4b, increase with increasing BST additive amount, where  $\varepsilon_2$  (photo-catalysis enhancement) ranges from ~100-275 and is much higher than  $\varepsilon_1$  (piezo-catalysis enhancement) which is less than 10, due to the weak efficiency of photocatalysis alone compared to the piezocatalytic reaction alone. For the best catalyst type, the highest level of enhancement for photo-piezo-catalysis is  $\varepsilon_2 = 275\%$ , where the BST additive amount is 100 wt%. The squeeze frequency, Figure 4c, also influences the piezo-catalytic reaction since it affects the generation of piezoelectrically induced electric charges, which can drive the subsequent electrochemical catalytic processes.<sup>30</sup> In this process, we compare the catalytic effect and enhancement under low-frequency mechanical squeezing at 0, 0.12, 0.38, and 0.71 Hz, as shown in Figure 4c and 4d. As expected, a higher squeeze frequency achieves a more desirable catalytic effect, and the photo-piezo-catalytic coupling effect exhibits a substantial increase with an increase of squeeze frequency. For various dye wastewater solution types including RhB, methyl green (MG), methyl blue (MB), methyl violet (MV) and methyl orange (MO), the catalytic reactions show differences in Figure 4e and 4f. After undergoing photo-piezo-catalysis within 90 min, the catalytic degradation ratio for RhB, MG, MB, MV and MO are 97.8%, 66.1%, 23.1%, 39.6%, and 3.3%, respectively. The degradation ratio of MG, MB, MV and MO dyes are much lower than RhB, which can be attributed to their disparate molecular structure, as shown in Table 1 of the Supplementary. The efficient photo-piezo-catalytic RhB degradation can be considered to the result of the de-ethylation process, while MB, MV and MO dyes contain C=N, N=N double bonds that are difficult to destroy, which causes weak degradation ratio for catalytic reactions. 31-33 In addition, the pH level affects the photo-piezo-catalytic coupling effect slightly, as shown in Figure S7c.

Mechanism for photo-piezo-catalytic coupling effect. As reported, the main active species during catalytic reactions are holes ( $h^+$ ), superoxide radicals ( $\bullet$ O<sup>2-</sup>) and hydroxyl radicals ( $\bullet$ OH),<sup>34</sup> so that trapping tests are illustrated in Figure S7d. Tertbutyl alcohol (TBA), p-benzoquinone (BQ), and ethylenediaminetetraacetic acid (EDTA) are the specific scavengers for  $\bullet$ OH,  $\bullet$ O<sup>2-</sup> and  $h^+$ , respectively.<sup>34,35</sup> Under the photo-piezo-catalytic processes, the effect of photo-piezo-catalytic coupling clearly shows a large decrease with the addition of TBA or BQ scavengers, and a small decrease when added with EDTA scavengers; this is in contrast to the process of photo-piezo-catalysis without any scavengers. Therefore we can assume that  $\bullet$ OH and  $\bullet$ O<sup>2-</sup> radicals are the most important active species, while  $h^+$  are less important species for photo-piezo-catalytic coupling effect.

A schematic of the photocatalytic effect alone, piezo-catalytic effect alone, and coupled photo-piezo-catalytic effect for dye degradation using ferro-/piezo-electric BST nanoparticles subjected to light

irradiation and/or regular mechanical squeezing are illustrated in Figure 5 and S8. As mentioned above, •OH and •O<sup>2</sup>- radicals play a significant role in the catalytic reactions, and their standard redox potentials (OH<sup>-</sup>/•OH and O<sub>2</sub>/•O<sub>2</sub><sup>-</sup>) are +1.90 V and -0.33 V versus NHE, respectively.<sup>36</sup> When there is no light irradiation and no regular mechanical squeezing, the BST nanoparticles remain in equilibrium with the solution at room temperature, where the top of the valence band (VB) and the bottom of the conduction band (CB) of the BST are +2.57 V and -0.50 V versus NHE, respectively.<sup>37</sup> The piezoelectric polarization ( $P_{pz}$ ) of the BST corresponds to a minimum, and there is only a small quantity of electric charges (holes and electrons) at the VB and CB via thermal emission. As a result of the high-rate recombination of electrons and electrons, there is very limited catalytic performance in this state.

For the photocatalytic effect alone, the system is subjected to irradiation by light, as shown in Figure S9. The quantity of electric charges increases sharply as a result of photo-emission; however only a small quantity of electric charges are able to move to the material surface in order to participate in electrochemical reactions due to the recombination of electron-hole pairs. As a result, under only light irradiation there is a limited amount of generated •O<sup>2</sup>- and •OH radicals that results in a weak level of photocatalytic dye degradation. For the piezo-catalytic effect alone, the reaction system is subjected to regular mechanical squeezing, as shown in Figure 5. The value of  $P_{pz}$  varies over time, and the piezocatalytic process can be divided into four states ( $P_{pz} = \min$ ,  $P_{pz} \rightarrow \max$ ,  $P_{pz} = \max$ ,  $P_{pz} \rightarrow \min$ ), which are illustrated in Figure 5a and  $5b_{1-3}$ . When the BST is subjected to regular mechanical squeezing,  $P_{pz}$ begins from a minimum and increases to a maximum, which breaks the equilibrium of piezoelectrically induced electric charges and associated screening charges. As a result, electron-hole pairs are driven to the material surface to compensate the charge unbalance.<sup>19</sup> The separated electron-hole pairs can then react with free oxygen molecules and hydroxyl ions to form •O2- and •OH radicals for piezo-catalytic dye degradation. When  $P_{pz}$  reaches a maximum, the piezoelectrically induced electric charges and screened charges gradually build to a new equilibrium. After that, the  $P_{pz}$  falls to a minimum and the amount of piezoelectrically induced electric charges decreases where the electron-hole pairs can be driven to the reverse side of the material, which leads to a same level of piezo-catalytic dye degradation. From Figure 5b<sub>1</sub> and 5b<sub>3</sub>, the orientation of the bending of the surface energy bands is related to the balance between the piezoelectrically induced charges and screened charges.<sup>40</sup> However, the electronhole pairs originate from thermal emission, and the limited amount of electron-hole pairs gained in this way continues to limit the efficiency of the catalytic dye degradation process.

For the coupled photo-piezo-catalytic effect, the reaction system is subjected to both irradiation by light and regular mechanical squeezing simultaneously. This coupling effect can be described by four states, as follows: (I)  $P_{pz} = \min$ , the piezoelectrically induced charges remain in equilibrium with

screened charges, where the electron-hole pairs are generated from thermal emission and photo-emission. (II)  $P_{\rm pz} \rightarrow {\rm max}$ , when BST is subjected to light irradiation and regular squeezing, a large amount of photo-generated and a small quantity of thermal-generated electron-hole pairs move to the material surface under the piezoelectric electric field to balance the piezoelectrically induced charges and the screened charges since the amount of piezoelectrically induced charges change with the value of  $P_{\rm pz}$ . (III)  $P_{\rm pz} = {\rm max}$ , the piezoelectrically induced charges re-establish an equilibrium with the screened charges. (IV)  $P_{\rm pz} \rightarrow {\rm min}$ , the piezoelectrically induced charges decrease with a decrease in piezoelectric polarization, and photo-generated and thermal-generated electric charges are driven to the reverse side of the particle compared to state (III). In summary, at the states (II) and (IV), electron-hole pairs are driven to the surface to participate in the following electrochemical processes for enhanced dye degradation. In summary, the above mechanism of the photo-piezo-catalytic coupling effect can be expressed as follows:

BST - PDMS 
$$\xrightarrow{\text{irradiation and squeeze}}$$
 BST - PDMS +  $e^- + h^+$  (5)

$$e^{-} + O_{2} \rightarrow \bullet O_{2}^{-} \tag{6}$$

$$h^+ + OH^- \rightarrow \bullet OH$$
 (7)

• 
$$O_2^- + \bullet OH + dye molecules \rightarrow dye degradation$$
 (8)

The photo-piezo-catalytic effect combines the advantages of increased number of generated electron-hole pairs and a piezoelectric field to achieve a higher efficiency in electron-hole separation, which thereby provides an enhanced catalytic dye degradation.

#### **Discussion**

In this work, an enhanced photo-piezo-catalytic coupling effect for dye wastewater degradation has been realized in a BST-PDMS porous foam under light irradiation and low-frequency mechanical squeezing, where the degradation efficiency reaches a high level of 97.8% and a performance enhancement of 275% was achieved in contrast to individual photocatalysis. The structure of the porous foam brings a series of advantages, these include the fact that the nanostructured piezoelectric catalysts can be tightly packed in a PDMS matrix to restrict secondary pollution, while maintaining ample contact with dye solutions for high efficiency degradation. In addition, the porous foam can be easily recycled and reused, where cyclic photo-piezo-catalytic testing of the BST-PDMS porous foam achieves a limited decrease in degradation efficiency after 10 repeated cycles of catalytic reactions from the 1<sup>st</sup> cycle of 97.8% to the 10<sup>th</sup> cycle of 92.7%. Such an excellent recycling performance is attributed to the fact that

piezoelectric material under low-frequency mechanical squeezing are not easily damaged compared to high-energy ultrasonic waves and resulting cavitation. The degradation efficiency and coupling evaluation have been evaluated for a variety of BST additive amounts, squeeze frequencies, dye types and pH levels to optimise the system. In addition, the proposed mechanism of the coupled photo-piezo-catalytic effect can be described as combining the advantages of increased generated electron-hole pairs due to the photovoltaic effect and the piezoelectric field that improves the electron-hole separation. Therefore, The BST-PDMS porous foam with photo-piezo-catalytic coupling for dye degradation offers a potential approach in wastewater degradation by using both solar energy and environmental low-frequency mechanical sources.

#### Methods

Preparation of BST nanoparticles. All starting chemicals were obtained commercially and used without further purification. The BST nanoparticles used in our experiment were synthesized by a conventional solid-state reaction. Initially, barium titanate (BaTiO<sub>3</sub>, 99.9%, AR) and strontium titanate (SrTiO<sub>3</sub>, 99.9%, AR) powders with a stoichiometric ratio of 7:3 were ball-milled in an alcohol medium for 24 h. The mixture was then dried at 70 °C and calcined at 1150 °C. Subsequently, the calcined products were reg-round and wet ball milled for 24 h to reduce the particle size. The BST nanoparticles were finally obtained after drying in air at 90 °C for 24 h.

**Fabrication of BST-PDMS porous foam.** An appropriate amount of as-prepared BST nanoparticles was added to a beaker containing pure PDMS, granulated sugar (pore-former) and curing agent, where the ratio of pure PDMS and curing agent was 10:1 in weight. After stirring evenly utilizing a glass bar, the mixture was transferred into a 3 cm-diameter cylindrical acrylic mold and then extruded by a suitable acrylic wafer. Thereafter, the mixture could be solidified when the temperature was increased to 70 °C for 3 h. In order to remove the granulated sugar for pore-formation, the cured mixture was placed in 500 mL deionized water under ultrasound excitation. Finally, the BST-PDMS porous foam was obtained after being dried in oven at 50 °C.

Characterization and measurements. The crystalline phase of the synthesized BST nanoparticles was characterized using an X-ray diffractometer (XRD, PANalytical X'pert3, the Netherlands) with Cu K $\alpha$  ( $\lambda$  = 1.5406 Å,  $2\theta$  = 10-80°). A field emission scanning electron microscope (FESEM, Hitachi SU8020, Japan) with an acceleration voltage of 5 kV was used to characterize the microstructure and morphology of the BST nanoparticles and as-prepared BST-PDMS porous foam. As-prepared BST nanoparticles were also characterized using atomic force microscopy (AFM, Bruker ICON, USA) in contact mode, where the topology, piezo-response amplitude and phase were characterized from recorded deformation signals when a 10 V voltage was applied.

Catalytic active experiments. The photo-catalytic, piezo-catalytic and photo-piezo-catalytic activities of the BST-PDMS porous foam were investigated by measuring the degradation of Rhodamine B (RhB) under irradiation and/or mechanical squeezing, respectively. In a typical measurement, 60 mL of 25 mg·L<sup>-1</sup> RhB and a BST-PDMS porous foam were placed in a 150 mL beaker. Prior to catalytic measurements, the porous foam and the RhB solution were processed to establish an adsorption-desorption equilibrium. During the photocatalytic experiment, a Xe-lamp with ultraviolet and visible components was used as the light source with an irradiation of 1 sun. During the piezo-catalytic experiment, a mechanical device was used to squeeze the porous foam at a regular and low frequency by connection to a tension meter (ZTS-50N, IMADA, Japan) attached to an electric vertical dynamometer machine (MX2-500N, IMADA, Japan). In addition, typical photo-piezo-catalysis experiment, the porous foam was simultaneously subjected to both irradiation and squeezing. At different time intervals, an appropriate amount of the reaction solution was collected, and the RhB concentration was analyzed by an UV-Vis spectroscopic measurement (Ultra-6600A, RIGOL, China).

#### References

- 1. Berg, D. et al. Energy without pollution. Science 170, 17-8 (1970).
- 2. Kabra, K. *et al.* Treatment of hazardous organic and inorganic compounds through aqueous-phase photocatalysis: a review. *Ind. Eng. Chem. Res.* **43**, 7683-7696 (2004).
- 3. Borgarello, E. *et al.* Photochemical cleavage of water by photocatalysis. *Nature* **289**, 158-160 (1981).
- 4. Fujishima, A. *et al.* Electrochemical photolysis of water at a semiconductor electrode. *Nature* **238**, 37-38 (1972).
- 5. Elimelech, M. *et al.* The future of seawater desalination: energy, technology, and the environment. *Science* **333**, 712-717 (2011).
- 6. Huang, H. *et al.* Two novel bi-based borate photocatalysts: crystal structure, electronic structure, photoelectrochemical properties, and photocatalytic activity under simulated solar light irradiation. *J. Phys. Chem. C* **117**, 22986-22994 (2013).
- 7. Qian, W. *et al.* Thermo-electrochemical coupling for room temperature thermocatalysis in pyroelectric ZnO nanorods. *Electrochem. Commun.* **81**, 124-127 (2017).
- 8. You, H. *et al.* Strong piezo-electrochemical effect of multiferroic BiFeO<sub>3</sub> square microsheets for mechanocatalysis. *Electrochem. Commun.* **79**, 55-58 (2017).
- 9. Chen, C. *et al.* Photocatalysis by titanium dioxide and polyoxometalate/TiO<sub>2</sub> cocatalysis. intermediates and mechanistic study. *Environ. Sci. Technol.* **38**, 329-337 (2004).
- 10. Banerjee, S. et al. New insights into the mechanism of visible light photocatalysis. J. Phys. Chem.

- *Lett.* **5**, 2543-2554 (2014).
- 11. Starr, M. B. *et al.* Coupling of piezoelectric effect with electrochemical processes. *Nano Energy* **14**, 296-311 (2015).
- 12. Zhang, Y. *et al.* Control of electro-chemical processes using energy harvesting materials and devices. *Chem. Soc. Rev.* **46**, 7757-7786 (2017).
- 13. Liang, Z. *et al.* Piezoelectric materials for catalytic/photocatalytic removal of pollutants: recent advances and outlook. *Appl. Cataly. B: Environ.* **241**, 256-269 (2019).
- 14. Xue, X. *et al.* Piezo-potential enhanced photocatalytic degradation of organic dye using ZnO nanowires. *Nano Energy* **13**, 414-422 (2015).
- 15. Tan, C. F. *et al.* Self-biased hybrid piezoelectric-photoelectrochemical cell with photocatalytic functionalities. *ACS Nano* 9, 7661–7670 (2015).
- 16. Li, H. D. *et al.* Enhanced ferroelectric-nanocrystal-based hybrid photocatalysis by ultrasonic-wave-generated piezophototronic effect. *Nano Lett.* **15**, 2372-2379 (2015).
- 17. Mushtaq, F. *et al.* Piezoelectrically enhanced photocatalysis with BiFeO<sub>3</sub> nanostructures for efficient water remediation. *iScience* **4**, 236-246 (2018).
- 18. Hu, C. *et al.* Coupling piezocatalysis and photocatalysis in Bi<sub>4</sub>NbO<sub>8</sub>X (X = Cl, Br) polar single crystals. *Adv. Funct. Mater.*, **30**, 1908168 (2019).
- 19. Qian, W. *et al.* Piezoelectric material-polymer composite porous foam for efficient dye degradation via the piezo-catalytic effect. *ACS Appl Mater Interfaces* **11**, 27862-27869 (2019).
- 20. Huang, K. *et al.* Significant polarization variation near room temperature of Ba<sub>0.65</sub>Sr<sub>0.35</sub>TiO<sub>3</sub> thin films for pyroelectric energy harvesting. *Sens. Actuators B* **169**, 208-212 (2012).
- 21. Basmajian, J. A. et al. Phase equilibria in the system BaTiO<sub>3</sub>-SrTiO<sub>3</sub>. J Am. Ceram. Soc. 40, 373-376 (1957).
- 22. Merz, W. J. Double hysteresis loop of BaTiO<sub>3</sub> at the curie point. *Phys. Rev.* **91**, 513-517 (1953).
- 23. Bhardwaj, A. *et al.* Enhanced photochemical reactivity at the ferroelectric phase transition in Ba<sub>1-</sub> <sub>x</sub>Sr<sub>x</sub>TiO<sub>3</sub>. *J. Am. Ceram. Soc.* **93**, 4129-4134 (2010).
- 24. Mocherla, P. S. V. *et al.* Tunable Bandgap in BiFeO<sub>3</sub> nanoparticles: the role of microstrain and oxygen defects. *Appl. Phys. Lett.* **103**, 022910 (2013).
- 25. Li, S. *et al.* Controlled fabrication of BiFeO<sub>3</sub> uniform microcrystals and their magnetic and photocatalytic behaviors. *J. Phys. Chem. C* **114**, 2903-2908 (2010).
- 26. Cardona, M. Optical Properties and band structure of SrTiO<sub>3</sub> and BaTiO<sub>3</sub>. *Phys. Rev.* **140**, 651-655 (1965).
- 27. Wemple, S. H. Polarization fluctuations and the optical-absorption edge in BaTiO<sub>3</sub>. *Phys. Rev. B* **2**, 2679-2689 (1970).

- 28. Yu, Y. *et al.* Dielectric properties of Ba<sub>1-x</sub>SrxTiO<sub>3</sub> ceramics prepared by microwave sintering. *Ceram. Int.* **39**, S335-S339 (2013).
- 29. Kohl, S. K. *et al.* Demonstration of absorbance using digital color image analysis and colored solutions. *J. Chem. Educ.* **83**, 4, 644 (2006).
- 30. You, H. *et al.* Harvesting the vibration energy of BiFeO<sub>3</sub> nanosheets for hydrogen evolution. *Angew. Chem. Int. Ed.* **58**, 11779-11784 (2019)
- 31. Testino, A. *et al.* Optimizing the photocatalytic properties of hydrothermal TiO<sub>2</sub> by the control of phase composition and particle morphology. A systematic approach. *J. Am. Chem. Soc.* **129**, 3564-3575 (2007).
- 32. Yang, X. *et al.* Mesoporous structure with size controllable anatase attached on silicate layers for efficient photocatalysis. *J. Phys. Chem. C* **113**, 19, 8243-8248 (2009).
- 33. Zhao, T. *et al.* Hierarchical Bi<sub>2</sub>O<sub>2</sub>CO<sub>3</sub> microspheres with improved visible-light-driven photocatalytic activity. *CrystEngComm* **13**, 4010-4017 (2011).
- 34. Xu, T. *et al.* Significant enhanced photocatalytic performance of ZnO via graphene hybridization and the mechanism study. *Appl. Catal. B* **101**, 382-387 (2011).
- 35. Yin, M. *et al.* Mechanism investigation of visible light-induced degradation in a heterogeneous TiO<sub>2</sub>/Eosin Y/Rhodamine B system. *Environ. Sci. Technol.* **43**, 8361-8366 (2009).
- 36. Wardman, P. Reduction potentials of one-electron couples involving free radicals in aqueous solution. *J. Phys. Chem.* **18**, 1637-1755 (1989).
- 37. Xu, X. *et al.* Pyro-catalytic hydrogen evolution by Ba<sub>0.7</sub>Sr<sub>0.3</sub>TiO<sub>3</sub> nanoparticles: harvesting cold-hot alternation energy near room-temperature. *Energy Environ. Sci.* **11**, 2198-2207 (2018).
- 38. Wu, J. *et al.* Effective enhancement of piezocatalytic activity of BaTiO<sub>3</sub> nanowires under ultrasonic vibration. *Nano Energy* **45**, 44-51(2018).
- 39. Rai, S. C. *et al.* Enhanced broad band photodetection through piezo-phototronic effect in CdSe/ZnTe core/shell nanowire array. *Adv. Electron. Mater.* **1**, 1400050 (2015).
- 40. Damjanovic, D. *et al.* Crystal orientation dependence of the piezoelectric  $d_{33}$  coefficient in tetragonal BaTiO<sub>3</sub> as a function of temperature. *Appl. Phys. Lett.* **80**, 652-654 (2002).

## Acknowledgments

This work was supported by the National Key R&D Program of China (Grant No. 2016YFA0202701), the National Natural Science Foundation of China (Grant No. 51472055, No. 61974170), External Cooperation Program of BIC, Chinese Academy of Sciences (Grant No. 121411KYS820150028), the 2015 Annual Beijing Talents Fund (Grant No. 2015000021223ZK32), Qingdao National Laboratory for

Marine Science and Technology (No. 2017ASKJ01), the University of Chinese Academy of Sciences (Grant No. Y8540XX2D2), and the "thousands talents" program for the pioneer researcher and his innovation team, China.

## **Author contributions**

Y.Y. and C. L. conceived the idea and supervised the research; S. X. and W. Q. fabricated the composite materials; S. X., W. Q., D. Z. and X. Z. carried out the device fabrication and the performance measurement; S. X., W. Q., X. Z., C. L., C. R. B. and Y. Y. analyzed the data and co-wrote the manuscript. All the authors read and revised the manuscript.

### **Additional information**

Supplementary Information accompanies this paper at http://www.nature.com/naturecommunications

Competing financial interests: The authors declare no competing financial interests.

**Reprints and permission** information is available online at http://npg.nature.com/reprintsandpermissions/

How to cite this article:

#### **FIGURES**

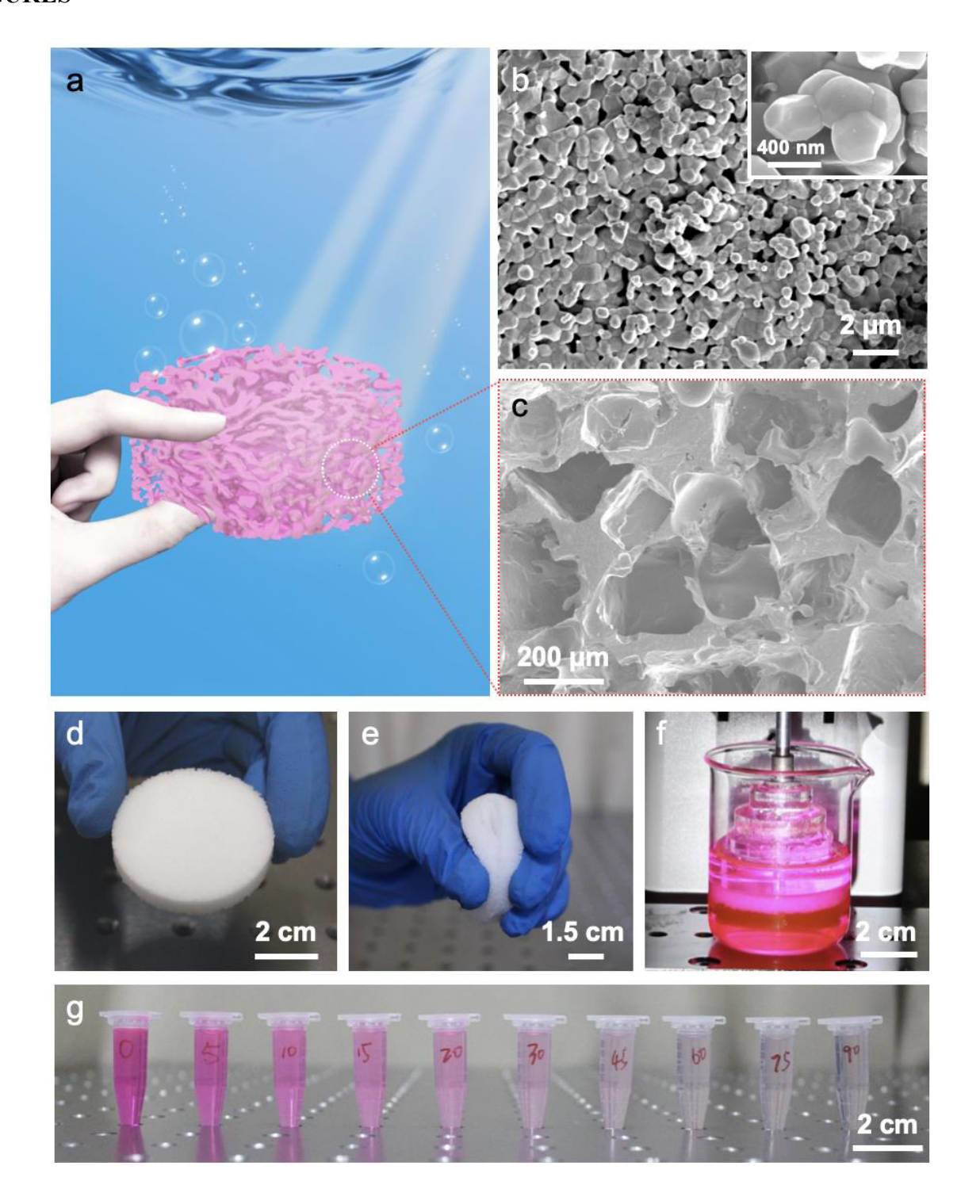


**Figure 1.** Characterization of BST-PDMS. (a) Schematic of porous foam during photo-piezo-catalysis. (b) SEM images of the prepared BST nanoparticles. (c) SEM image of the BST-PDMS porous foam. (d, e) Photograph of the BST-PDMS porous foam. (f) Photograph of the BST-PDMS porous foam during the photo-piezo-catalysis process. (g) Photograph of efficient RhB dye degradation during 90 min of photo-piezo-catalysis.

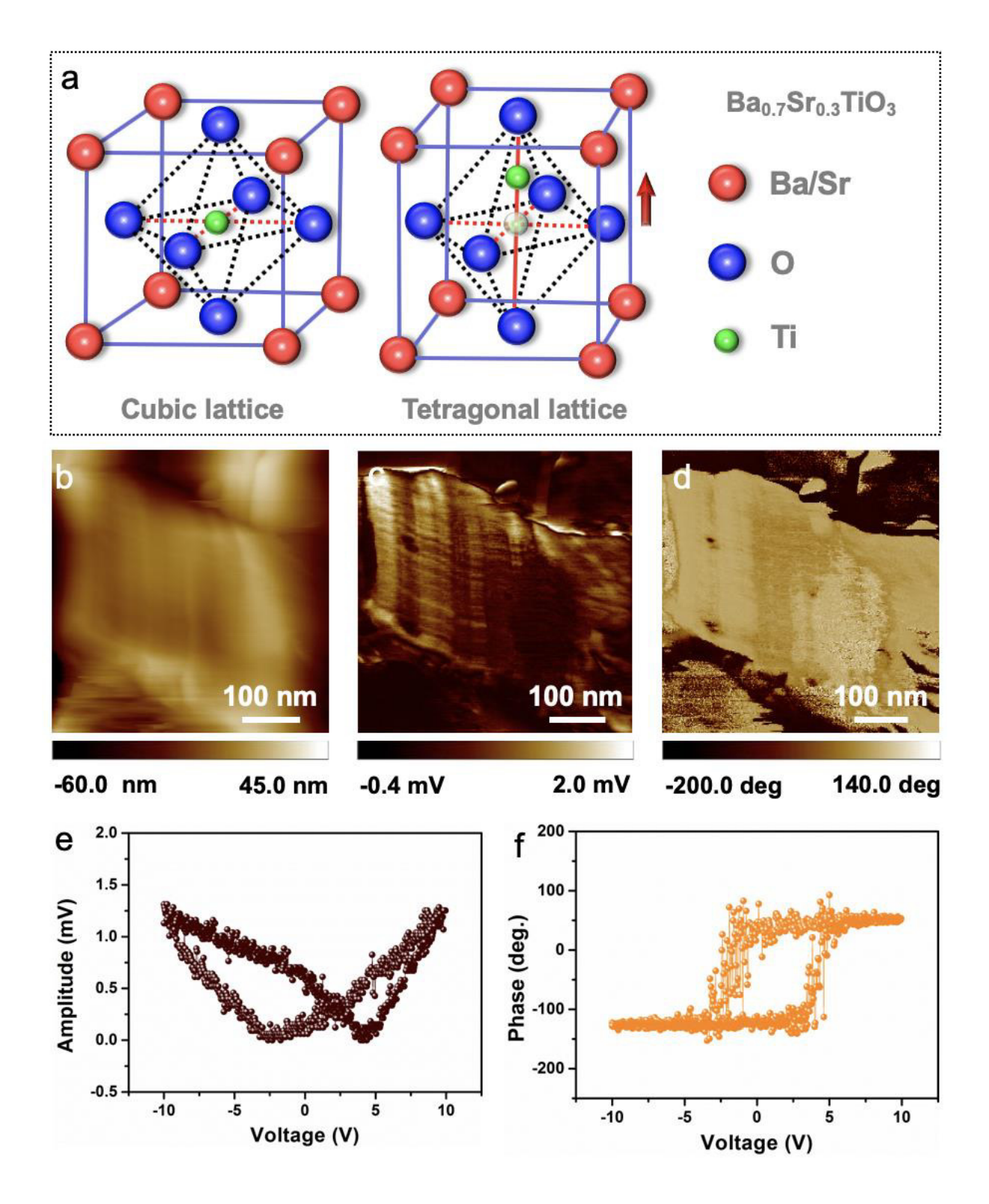


**Figure 2.** Piezoelectric and ferroelectric characterization of BST. (a) Origin of spontaneous polarization in ferro-/piezo-electric BST. (b) AFM morphology of BST nanoparticles. (c) PFM amplitude of BST nanoparticles. (d) Phase image of BST nanoparticles. (e, f) Ferroelectric hysteresis loops of BST nanoparticles.

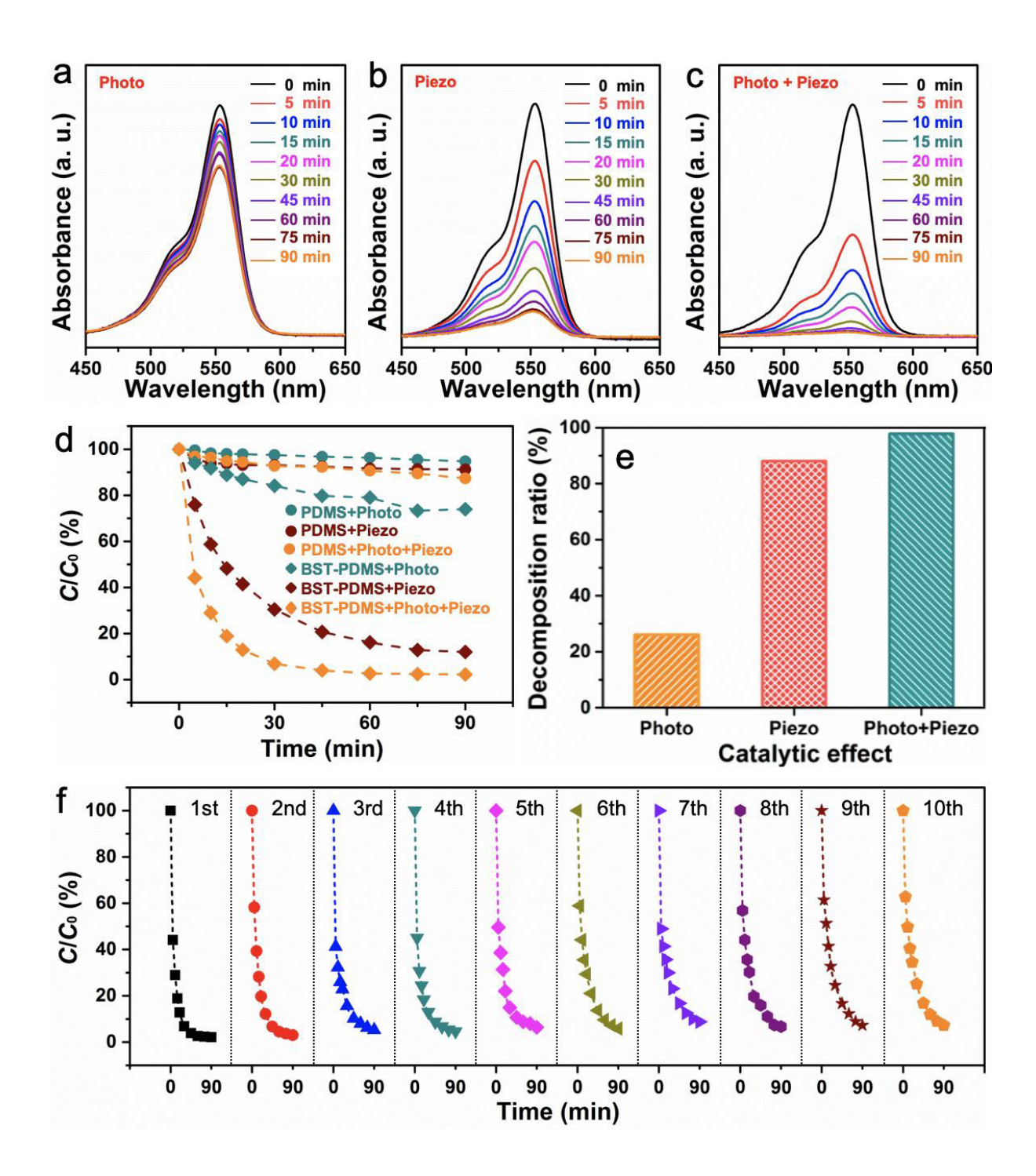


**Figure 3.** Catalytic activity of the BST-PDMS porous foam. (**a**, **b**, **c**) Absorbance of RhB solution in BST-PDMS under light irradiation only (a), under low-frequency mechanical squeezing only (b), and under a combination of light irradiation and low-frequency mechanical squeezing (c). (**d**) Catalytic activity of RhB solution in the presence of pure PDMS and BST-PDMS. (**e**) Dependence of decomposition ratio on various catalysis in BST-PDMS. (**f**) Recycling of BST-PDMS during 10 photopiezo-catalytic cycles.

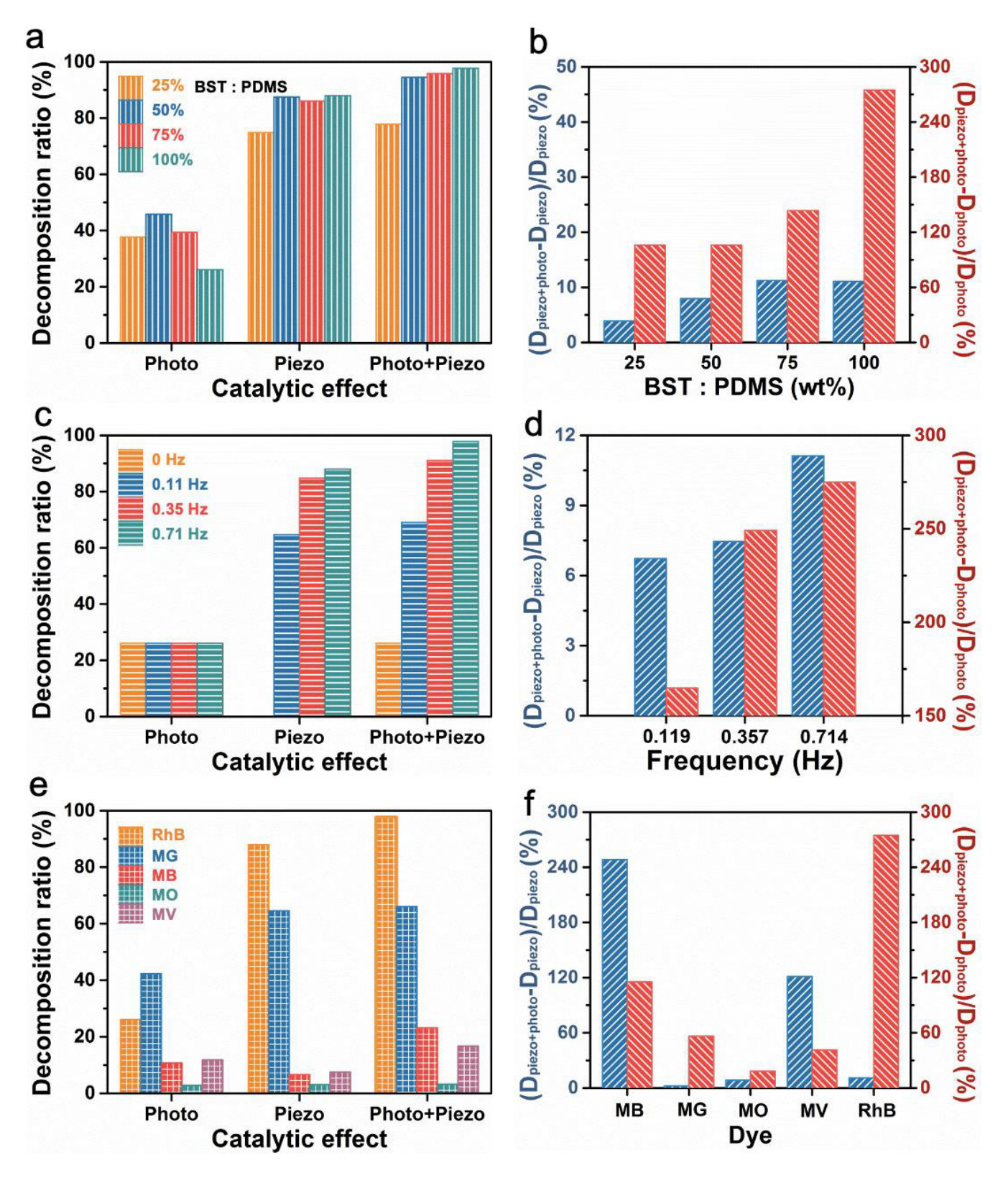


**Figure 4.** Dependence of catalytic coupling activity on different conditions. (**a**, **b**) Dependence of catalytic coupling activity on the amount of BST. (**c**, **d**) Dependence of catalytic coupling activity on squeeze frequency. (**e**, **f**) Dependence of catalytic coupling activity on type of dye solution.

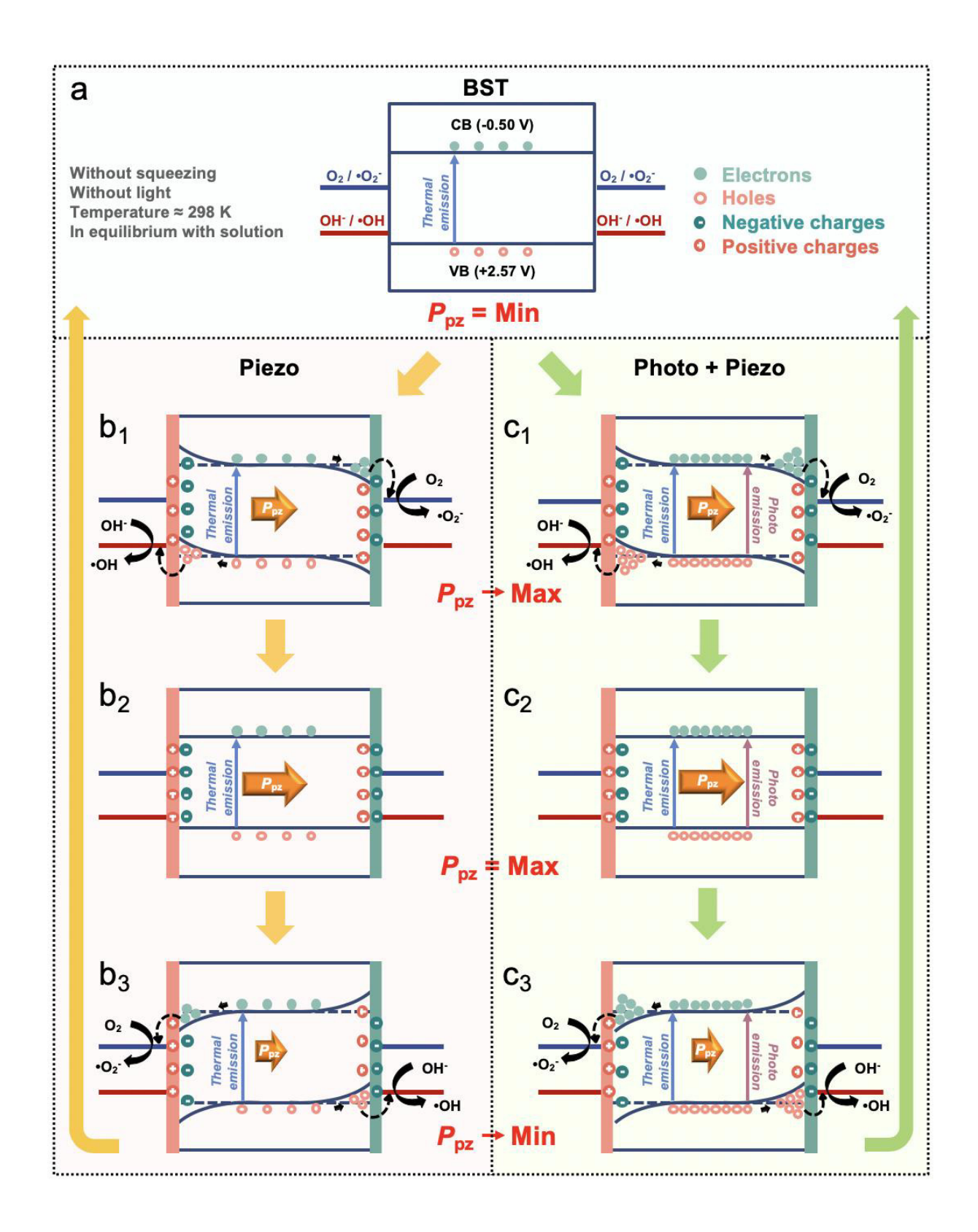


**Figure 5.** Schematic of the photo-piezo-catalytic coupling effect in BST-PDMS. (a) Energy band of BST in equilibrium with the surrounding solution. (b) Energy bands of BST during piezo-catalysis. (c) Energy bands of BST during photo-piezo-catalysis.